


High-Dimensional Entanglement-Enabled Holography

Ling-Jun Kong,^{*} Yifan Sun,^{*} Furong Zhang, Jingfeng Zhang, and Xiangdong Zhang^{✉†}
 Key Laboratory of Advanced Optoelectronic Quantum Architecture and Measurements of Ministry of Education,
 Beijing Key Laboratory of Nanophotonics and Ultrafine Optoelectronic Systems, School of Physics,
 Beijing Institute of Technology, 100081 Beijing, China

 (Received 28 August 2022; accepted 9 January 2023; published 2 February 2023)

As an important imaging technique, holography has been realized with different physical dimensions of light, including polarization, wavelength, and time. Recently, quantum holography has been demonstrated by utilizing polarization entangled state with the advantages of high robustness and enhanced spatial resolution, comparing with classical holography. However, the polarization is only a two-dimensional degree of freedom, which greatly limits the capacity of quantum holography. Here, we propose a method to realize high-dimensional quantum holography by using high-dimensional orbital angular momentum (OAM) entanglement. A high-capacity OAM-encoded quantum holographic system can be obtained by multiplexing a wide range of OAM-dependent holographic images. Proof-of-principle experiments with four- and six-dimensional OAM entangled states have been implemented and verify the feasibility of our idea. Our experimental results also demonstrate that the high-dimensional quantum holography shows a high robustness to classical noise. What is more, the level of security of the holographic imaging encryption system can be greatly improved in our high-dimensional quantum holography.

DOI: [10.1103/PhysRevLett.130.053602](https://doi.org/10.1103/PhysRevLett.130.053602)

The concept of holography was first introduced by Gabor [1,2]. Following the pioneering work of Gabor, Leith and Upatnieks applied the principle of holography to free-space optical beams with the advent of the laser [3], and Brown and Lohman invented the computer-generated hologram [4]. Now, holography has been implemented with x rays [5], electron beams [1], or neutron beams [6], and has become an essential tool of modern optics of many applications for three-dimensional displays [7–10], microscopy [11,12], optical encryption [13,14], information storage [15], generation of topological structures [16–19], and so on. To date, the different physical dimensions of light, including wavelength [20–24], time [25,26], and polarization [27,28] have been utilized to carry independent information for increasing the capacity of holographic systems.

On the other hand, holography has been introduced into the quantum optics [29–32] and observed with the polarization entangled state [33]. Information is encoded into the polarization state, allowing us to image through dynamic phase disorder and even in the presence of strong classical noise with enhanced spatial resolution compared with classical coherent holographic systems. However, polarization is a two-dimensional degree of freedom, which greatly limits the information capacity of the quantum holography. If high-dimensional quantum holography can be realized, the capacity will be further improved. Recently, orbital angular momentum (OAM) [34–40] has been introduced into the holographical system for encoding information. By using strong OAM selectivity in the

spatial-frequency domain, high-dimensional OAM holography with high capacity has been realized [41,42]. However, it is still a great challenge to introduce the strong OAM selectivity method into the quantum holographic system, achieve the high-dimensional OAM entanglement holography, and increase the information capacity of the quantum holography.

In this Letter, we introduce the high-dimensional OAM entangled states into the holographic imaging and propose a method to realize the high-dimensional quantum holography. By multiplexing a wide range of OAM-dependent holographic images and using a strong OAM selectivity method, we can obtain a high capacity OAM-encoded quantum holographic system. We have carried out the proof of principle experiment and verified the feasibility of the high-dimensional quantum holography and high capacity OAM-encoded quantum holographic system. The introduction of entanglement allows us to image even in the presence of strong classical noise. Our results also show that the level of security of the holographic imaging encryption system can be greatly improved by using the high-dimensional quantum entangled state.

Quantum OAM holography.—The arrangement of our high-dimensional quantum OAM holographic scheme is illustrated in Fig. 1(a). Photon pairs entangled in high-dimensional OAM are produced by pumping a β -barium borate (BBO) crystal under type I spontaneous parametric down-conversion. The high-dimensional OAM entangled state of the photon pair is described as $|\Psi\rangle = \sum_{l=-\infty}^{l=+\infty} c_l |l\rangle_A | -l\rangle_B$. Here, $|l\rangle$ denotes a state of photon

with an OAM of $l\hbar$, subscript $A(B)$ labels the optical path- $A(B)$, c_l represents the amplitude distribution of the l -th-order OAM state. Experimental data for certifying the high-dimensional OAM entangled source is offered in Sec. 1 of Supplemental Material [43]. Lenses $L1$ and $L2$ consist of a $4f$ system and image the plane of the BBO on the spatial light modulators, SLM- A and SLM- B . After interacting with the SLM- A , photon A is coupled into a single mode fiber (SMF) with collecting lenses (Lc_1 and Lc_2) and detected by a single photon detector ($D-A$). Because only the fundamental Gaussian mode state can be coupled into the SMF, the SLM- A and SMF are together used for projecting an OAM state (represented by $|x\rangle$) into $|0\rangle$. Therefore, the decoding operator of SLM- A can be described as $\hat{P}_A = |0\rangle_A \langle x|_A$. The SLM- B is used for displaying the holographic phase pattern and its function for photon B is described by an operator \hat{P}_B^H . After interacting with the SLM- B and an optical Fourier transformation operated by lens Lf , the photon B is collected by a multimode fiber (MMF) and detected by another single photon detector ($D-B$). The input end of the MMF scan in the Fourier plane of Lf . Thus, the holographic image with coincidence measurement between $D-A$ and $D-B$ is calculated as

$$H_i = |f\{\hat{P}_B^H(\langle 0|_A \hat{P}_A |\Psi\rangle)\}|^2. \quad (1)$$

Here, $f\{\cdot\}$ represents the Fourier transformation.

The superposition of various OAM states makes it impossible to recognize the image carried by each kind of OAM state directly. To realize the high-dimensional quantum OAM holography, we introduce a strong OAM-selective method for the high-dimensional OAM entangled states. The OAM-selective hologram is obtained by encoding an OAM state $|l_e\rangle$ onto an OAM-preserved hologram, which is generated by multiplying a target image with a sampling array (see Sec. 2 in Supplemental Material [43] for details). An example is shown in the top side of Fig. 1(a), where the target image is the letters “BIT”, the phase distribution of the OAM-preserved hologram is described with φ and $l_e = 1$. The OAM-selective hologram will be displayed on the SLM- B . In such a case, the function of the operator for photon B is expressed as $\hat{P}_B^H = e^{j\varphi} |l_e + l\rangle_B \langle l|_B$. With setting the OAM decoding operator with $\hat{P}_A = |0\rangle_A \langle 3|_A$, $|0\rangle_A \langle 2|_A$, $|0\rangle_A \langle 1|_A$, $|0\rangle_A \langle -1|_A$, $|0\rangle_A \langle -2|_A$, or $|0\rangle_A \langle -3|_A$ by displaying the corresponding phase patterns on the SLM- A , the quantum OAM-selective holographic images can be calculated by Eq. (1). Experiment has been carried out. The experimental results are given in Fig. 1(b), and the corresponding simulation results are shown in Sec. 3 of Supplemental Material [43]. Because the encoded OAM state in the OAM-selective hologram is $|1\rangle$, only the given OAM decoding operator $\hat{P}_A = |0\rangle_A \langle 1|_A$ can convert each pixel of the holographic image into the Gaussian mode as

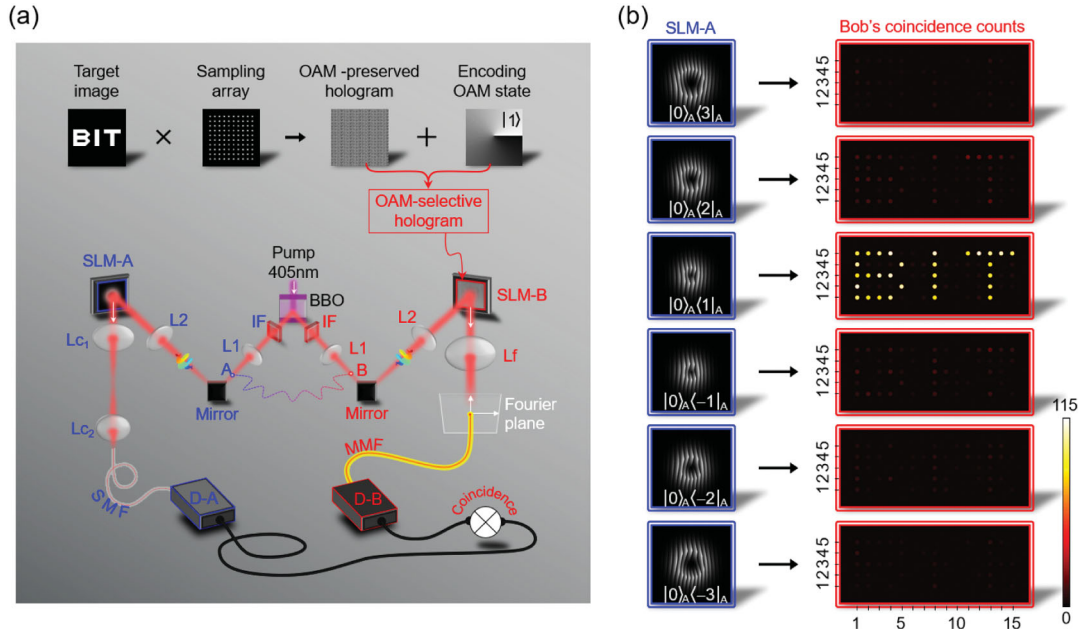


FIG. 1. OAM entanglement-enabled quantum holography. (a) The schematic of setup. IF, interference filter centred at 810 ± 3 nm; SLM- A/B , spatial light modulator; SMF, single mode fiber; MMF, multimode fiber with core diameter $25 \mu\text{m}$. $D-A/B$ single photon detectors; Lc/Lf , lens. Top side shows the design of the OAM preserved and OAM-selective hologram (see Sec. 2 in Supplemental Material [43] for details). (b) Quantum OAM-selective holographic images reconstructed with coincidence measurement by implementing the OAM decoding operators $\hat{P}_A = |0\rangle_A \langle 3|_A$, $|0\rangle_A \langle 2|_A$, $|0\rangle_A \langle 1|_A$, $|0\rangle_A \langle -1|_A$, $|0\rangle_A \langle -2|_A$, and $|0\rangle_A \langle -3|_A$. There are $15 \times 5 = 75$ pixels in each reconstructed holographic image. Coincidence measurement for each pixel takes 15 s.

$\hat{P}_B^H(\langle 0|_A \hat{P}_A |\Psi\rangle) \propto \hat{P}_B^H|-1\rangle_B = e^{i\varphi}|0\rangle_B$. In the OAM-selective holographic experiment, only the Gaussian mode contributes to the reconstruction of holographic image (see Sec. 4 in Supplemental Material [43] for details). It is seen clearly that the OAM-selective holographic image can be reconstructed only for $\hat{P}_A = |0\rangle_A \langle 1|_A$ with signal-to-noise ratio (SNR) ~ 15.8 . The agreements between experimental and theoretical results are very good, which means that the high-dimensional OAM entanglement holography has been realized.

Quantum OAM-multiplexing holography.—Since different OAM eigenstates are orthogonal to each other, the corresponding OAM-selective hologram can be designed according to each OAM state to encode the information independently. When these OAM-selective holograms are combined, OAM multiplexing holograms can be generated. Then, we can obtain a high capacity OAM-encoded quantum holographic system by multiplexing a wide range of OAM-dependent holographic images. The multiplexing approach is illustrated in Fig. 2(a). There are a series of target images, letters $O, \dots, A, \dots, M, \dots$. The OAM-preserved hologram of each target image is generated by multiplying it with a sampling array. Then, the OAM-selective holograms are obtained by encoding OAM states $|l_1\rangle, \dots, |l_i\rangle, \dots, |l_j\rangle, \dots$ onto the OAM-preserved holograms. Finally, the OAM-multiplexing hologram is obtained by combining all OAM-selective holograms. Because the property of OAM states will be well maintained in each pixel of the reconstructed holographic images, incident OAM states can be used to reconstruct different holographic images from an OAM-multiplexing hologram. Thus, different target images can be reconstructed by using the OAM decoding operator with $\hat{P}_A = |0\rangle_A \langle l_1|_A, \dots, |0\rangle_A \langle l_i|_A, \dots, |0\rangle_A \langle l_j|_A, \dots$, respectively. Then, quantum holography with high capacity has been realized. The proof-of-principle experiment with four- and six-dimensional OAM entangled states has been carried out. The experimental results for the four-dimensional condition are offered in Sec. 4.4 of Supplemental Material [43]. The experimental results for the six-dimensional case are shown in Fig. 2(b). Here, six target images are letters O, A, M, E, Q , and H . Six encoding OAM states are $|3\rangle, |2\rangle, |1\rangle, |-1\rangle, |-2\rangle$, and $|-3\rangle$. The images of letters O, A, M, E, Q , and H can be obtained by using the OAM decoding operator of $\hat{P}_A = |0\rangle_A \langle 3|_A, |0\rangle_A \langle 2|_A, |0\rangle_A \langle 1|_A, |0\rangle_A \langle -1|_A, |0\rangle_A \langle -2|_A$, and $|0\rangle_A \langle -3|_A$, with SNR $\sim 8.8, 9.9, 10.4, 9.3, 9.4$, and 6.8 , respectively. The smaller SNRs for letters O and H are due to the smaller coincidence count rates of $|3\rangle_A |-3\rangle_B$ and $|-3\rangle_A |3\rangle_B$ (see experimental data offered in Sec. 1 of Supplemental Material [43]). Although we only give the four- and six-dimensional cases, from these experimental results and the simulation results for ten-dimensional case (offered in Sec. 4.4 of Supplemental Material [43]), it can be seen that higher dimensional quantum OAM holography is also

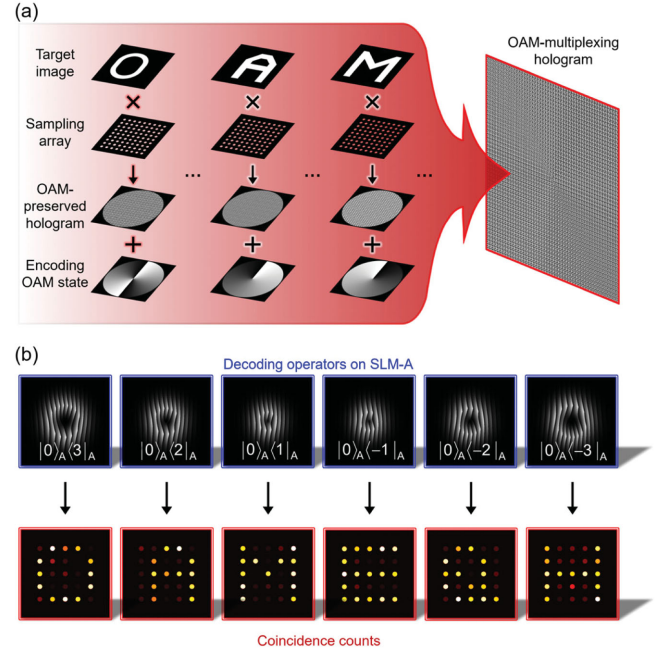


FIG. 2. Principle of quantum OAM-multiplexing holography. (a) Generation of an OAM-multiplexing hologram. (b) Experimental reconstructions of holographic images based on the OAM projective measurement operators $\hat{P}_A = |0\rangle_A \langle 3|_A, |0\rangle_A \langle 2|_A, |0\rangle_A \langle 1|_A, |0\rangle_A \langle -1|_A, |0\rangle_A \langle -2|_A$, and $|0\rangle_A \langle -3|_A$. There are $5 \times 5 = 25$ pixels and the coincidence measurement of each pixel takes 10 s.

feasible and the results will be similar. All these results prove the feasibility of quantum OAM-multiplexing holography.

Robustness of quantum OAM holography.—One of the advantages of quantum holography is its robustness to classical noise, as demonstrated for amplitude objects [49,50]. To test such an effect, we illuminate white light of a lamp as classical noise in the experiment of quantum OAM holography (see Sec. 5 in Supplemental Material [43] for details). The experimental results for reconstructing the OAM-selective holographic images are given in Fig. 3(a). It is shown clearly that the encoded image (letters “BIT”) can be accurately reconstructed for $\hat{P}_A = |0\rangle_A \langle 1|_A$ in the presence of classical stray light, with only a lower SNR compared to the case without stray light as shown in Fig. 1(b). In contrast, when we use a single photon, instead of entangled photons, to reconstruct the holographic image (see Sec. 5 in Supplemental Material [43] for details), the experimental results are provided in Fig. 3(b). The images become too vague to tell the letters, no matter what kind of OAM state is used. In the quantum OAM holographic system, the counts of coincidence measurement are related to the counts of each detector ($D-A$ and $D-B$) and their time correlation. The classical noise greatly increases the counts of $D-A$ and $D-B$, but slightly increases the counts of coincidence measurements because the counts coming from the classical noise do not have time correlation.

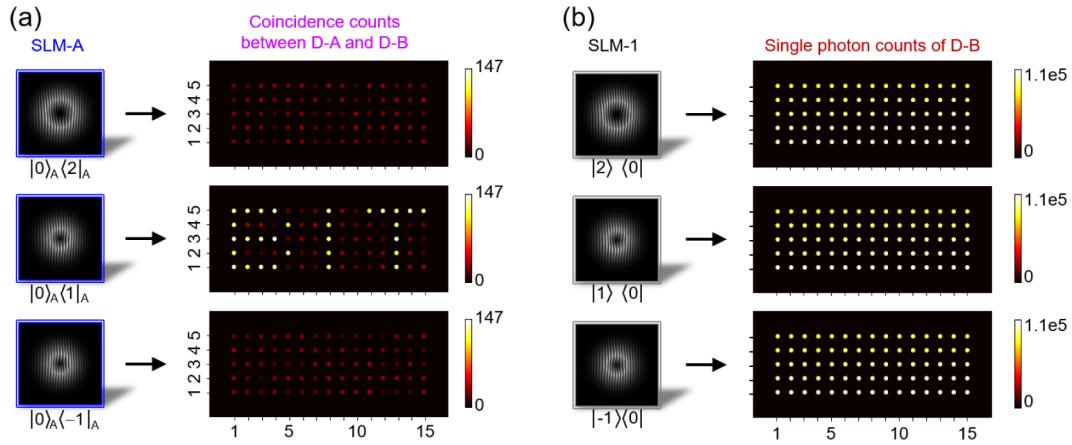


FIG. 3. Quantum OAM-selective holography in the presence of classical noise. (a) OAM-selective holographic images measured with quantum OAM holographic systems. (b) OAM-selective holographic images measured with classical OAM holographic systems.

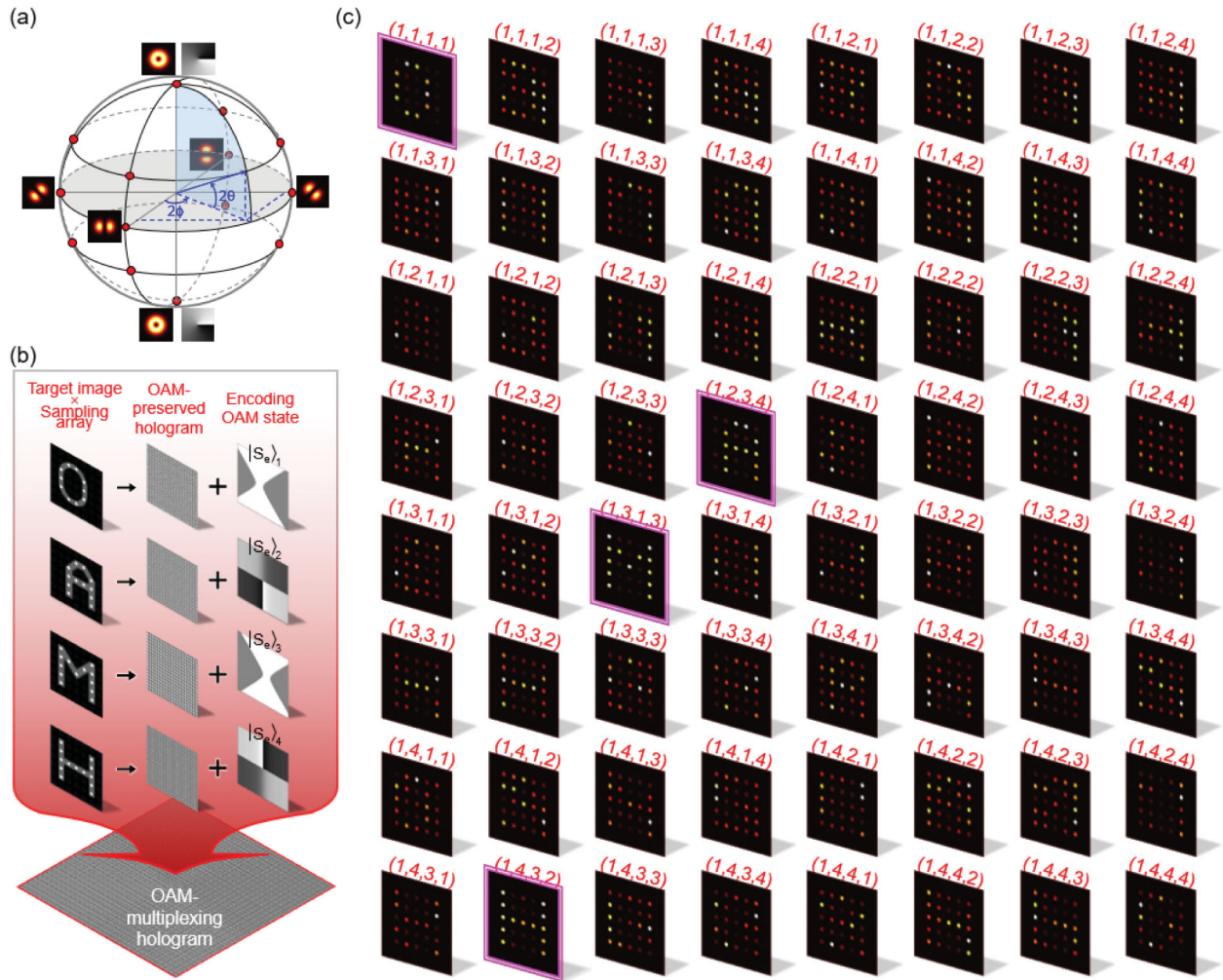


FIG. 4. Entanglement-enabled holography for high-security holographic imaging encryption. (a) Poincaré sphere composed of OAM states $|1\rangle$ and $|-1\rangle$. Its north and south poles represent the $|1\rangle$ and $|-1\rangle$. Any superposition state of $|1\rangle$ and $|-1\rangle$ can be represented by a point on the Poincaré sphere. (b) Design of multiplexing hologram based on OAM superposition states and its corresponding OAM-multiplexing hologram displaying on SLM-B. (c) Experimental OAM-selective holographic images for different decoding operators implemented with SLM-A.

The phenomena are similar to the case for the polarization entanglement-enabled quantum holography [33].

Entanglement-enabled holography for higher level security of holographic imaging encryption.—What is exciting is that the quantum OAM-selective holography enables an imaging encryption strategy with a higher level of security compared with that based on classical one [41]. As is well known, a classical bit would have to be in the bases state 0 or 1. However, a qubit is allowed to be in a coherent superposition of its basis state. Therefore, if one employs a superposition state as the key to encrypt a text, searching for the key in the corresponding state space (Hilbert space) would be much harder than that for a key encoded by bits in its finite state space. Here, we take the OAM states $|1\rangle$ and $|-1\rangle$ as an example. In the first-order OAM Poincaré sphere as shown in Fig. 4(a), $|1\rangle$ and $|-1\rangle$ are located at north and south poles, respectively [51,52]. Any state of superposition of $|1\rangle$ and $|-1\rangle$ can be described with a point on the Poincaré sphere, which is located by two angle parameters $\theta \in [-\pi/4, \pi/4]$ and $\phi \in [0, \pi]$. In our quantum OAM holographic system, the information can be encoded with any point on the Poincaré sphere in principle, which implies that one has to guess the key among infinite number of possible states if no prior knowledge of the encryption is available. For high-dimensional entangled states, the situation is similar. More discussion has been offered in Sec. 6 in Supplemental Material [43].

To verify the feasibility of entanglement-enabled holography for quantum imaging encryption, the experiments based on four-dimensional OAM entangled states have been done. As shown in Fig. 4(b), four OAM-preserved holograms are obtained by multiplying four target images (letters *O*, *A*, *M*, and *H*) with a sampling array, respectively. Then, four OAM superposition states, $|S_e\rangle_1 = (|-2\rangle + |-1\rangle + |2\rangle + |1\rangle)/2$, $|S_e\rangle_2 = (|-2\rangle + j|-1\rangle - |2\rangle - j|1\rangle)/2$, $|S_e\rangle_3 = (|-2\rangle - |-1\rangle + |2\rangle - |1\rangle)/2$, and $|S_e\rangle_4 = (|-2\rangle - j|-1\rangle - |2\rangle + j|1\rangle)/2$, are encoded into the OAM-preserved holograms for generating four OAM-selective holograms, respectively. The OAM-multiplexing hologram is achieved by combining these OAM-selective holograms and displays on the SLM-B. Figure 4(c) displays the experimental results of OAM-selective holographic images for 64 kinds of decoding operators. The decoding operators are implemented by the SLM-A, which are described as $\hat{P}_A = |0\rangle_A [e^{-j\pi(\alpha_1-1)/2} \langle -2|_A + e^{-j\pi(\alpha_2-1)/2} \langle -1|_A + e^{-j\pi(\alpha_3-1)/2} \langle 2|_A + e^{-j\pi(\alpha_4-1)/2} \langle 1|_A]/2$. The values of parameters $(\alpha_1, \alpha_2, \alpha_3, \alpha_4)$ are listed on each reconstructed OAM-selective holographic image. The images of letters *O*, *A*, *M*, and *H* can be decoded with $(\alpha_1, \alpha_2, \alpha_3, \alpha_4) = (1, 1, 1, 1)$, $(1, 2, 3, 4)$, $(1, 3, 1, 3)$, and $(1, 4, 3, 2)$ (marked with the frames of purple line) with SNR = 11.3, 9.4, 11.5, and 10.8, respectively. These results demonstrate that only when one knows the exact expression of the superposition state used for imaging

encryption, can he or she obtain the information of the encrypted four letters.

In conclusion, we have presented a way to realize the high-dimensional quantum holography based on high-dimensional OAM entangled states. Because different OAM eigenstates are orthogonal to each other, each OAM state can be implemented as an independent information carrier. Therefore, we can obtain a high-capacity quantum holographic system by multiplexing a wide range of OAM-dependent holographic images. Proof-of-principle experiment with four- and six-dimensional OAM entangled states has been carried out and verified the feasibility of the high-dimensional OAM quantum holography and high capacity quantum multiplex holography. Comparing with classical holography, quantum holography has practical advantages. The introduction of entanglement can effectively reduce the impact of classical noise, which leads to achieving decryption in the presence of strong noise. The use of the superposition state leads to more states being able to be selected for encoding information. Therefore, the level of security can be greatly improved in comparison with the classical one. At present, OAM entangled states with dozens of dimensions can be generated [53,54]. If quantum OAM holography with dozens of dimensions can be obtained based on our method, the capacity of quantum holographic imaging is greatly improved, and the security of quantum holographic imaging encryption can be improved to an unprecedented level.

This work was supported by the National Key R & D Program of China under Grant No. 2022YFA1404900, National Natural Science Foundation of China (12004038 and 11904022).

*These authors contributed equally to this work.

†Corresponding author.
zhangxd@bit.edu.cn

- [1] D. Gabor, A new microscopic principle, *Nature (London)* **161**, 777 (1948).
- [2] D. Gabor, Holography, 1948–1971, *Science* **177**, 299 (1972).
- [3] E. N. Leith and J. Upatnieks, Reconstructed wavefronts and communication theory, *J. Opt. Soc. Am.* **52**, 1123 (1962).
- [4] B. R. Brown and A. W. Lohmann, Complex spatial filtering with binary masks, *Appl. Opt.* **5**, 967 (1966).
- [5] W. L. Bragg, The X-ray microscope, *Nature (London)* **149**, 470 (1942).
- [6] B. Sur, R. B. Rogge, R. P. Hammond, V. N. P. Anghel, and J. Katsaras, Atomic structure holography using thermal neutrons, *Nature (London)* **414**, 525 (2001).
- [7] P.-A. Blanche *et al.*, Holographic three-dimensional telepresence using large-area photorefractive polymer, *Nature (London)* **468**, 80 (2010).
- [8] L. Huang *et al.*, Three-dimensional optical holography using a plasmonic metasurface, *Nat. Commun.* **4**, 2808 (2013).

- [9] K. Wakunami, P.-Y. Hsieh, R. Oi, T. Senoh, H. Sasaki, Y. Ichihashi, M. Okui, Y.-P. Huang, and K. Yamamoto, Projection-type see-through holographic three-dimensional display, *Nat. Commun.* **7**, 12954 (2016).
- [10] G. Makey, Ö. Yavuz, D. K. Kesim, A. Turnalı, P. Elahi, S. Ilday, O. Tokel, and F. Ö. Ilday, Breaking crosstalk limits to dynamic holography using orthogonality of high-dimensional random vectors, *Nat. Photonics* **13**, 251 (2019).
- [11] P. Marquet, B. Rappaz, P. J. Magistretti, E. Cuche, Y. Emery, T. Colomb, and C. Depeursinge, Digital holographic microscopy: A noninvasive contrast imaging technique allowing quantitative visualization of living cells with subwavelength axial accuracy, *Opt. Lett.* **30**, 468 (2005).
- [12] J. Rosen and G. Brooker, Non-scanning motionless fluorescence three-dimensional holographic microscopy, *Nat. Photonics* **2**, 190 (2008).
- [13] P. Refregier and B. Javidi, Optical image encryption based on input plane and Fourier plane random encoding, *Opt. Lett.* **20**, 767 (1995).
- [14] W. Chen, B. Javidi, and X. Chen, Advances in optical security systems, *Adv. Opt. Photonics* **6**, 120 (2014).
- [15] J. F. Heanue, M. C. Bashaw, and L. Hesselink, Volume holographic storage and retrieval of digital data, *Science* **265**, 749 (1994).
- [16] H. Larocque, D. Sugic, D. Mortimer, A. J. Taylor, R. Fickler, R. W. Boyd, M. R. Dennis, and E. Karimi, Reconstructing the topology of optical polarization knots, *Nat. Phys.* **14**, 1079 (2018).
- [17] L. Wang, W. Zhang, H. Yin, and X. Zhang, Ultrasmall optical vortex knots generated by spin-selective metasurface holograms, *Adv. Opt. Mater.* **7**, 1900263 (2019).
- [18] X. Guo, P. Li, J. Zhong, S. Liu, B. Wei, W. Zhu, S. Qi, H. Cheng, and J. Zhao, Tying polarization-switchable optical vortex knots and links via holographic all-dielectric metasurfaces, *Laser Photonics Rev.* **14**, 1900366 (2020).
- [19] L.-J. Kong, W. Zhang, P. Li, X. Guo, J. Zhang, F. Zhang, J. Zhao, and X. Zhang, High capacity topological coding based on nested vortex knots and links, *Nat. Commun.* **13**, 2705 (2022).
- [20] X. Li *et al.*, Athermally photoreduced graphene oxides for three-dimensional holographic images, *Nat. Commun.* **6**, 6984 (2015).
- [21] M. Ozaki, J. Kato, and S. Kawata, Surface-plasmon holography with white-light illumination, *Science* **332**, 218 (2011).
- [22] X. Li, L. Chen, Y. Li, X. Zhang, M. Pu, Z. Zhao, X. Ma, Y. Wang, M. Hong, and X. Luo, Multicolor 3D meta-holography by broadband plasmonic modulation, *Sci. Adv.* **2**, e1601102 (2016).
- [23] Y. Bao, Y. Yu, H. Xu, C. Guo, J. Li, S. Sun, Z.-K. Zhou, C.-W. Qiu, and X.-H. Wang, Full-colour nanoprint-hologram synchronous metasurface with arbitrary hue-saturation-brightness control, *Light Sci. Appl.* **8**, 95 (2019).
- [24] K. T. P. Lim, H. Liu, Y. Liu, and J. K. W. Yang, Holographic colour prints for enhanced optical security by combined phase and amplitude control, *Nat. Commun.* **10**, 25 (2019).
- [25] X. A. Shen, A.-D. Nguyen, J. W. Perry, D. L. Huestis, and R. Kachru, Time-domain holographic digital memory, *Science* **278**, 96 (1997).
- [26] A. Tikan, S. Bielawski, C. Szwarz, S. Randoux, and P. Suret, Single-shot measurement of phase and amplitude by using a heterodyne time-lens system and ultrafast digital time-holography, *Nat. Photonics* **12**, 228 (2018).
- [27] J. P. Balthasar Mueller, N. A. Rubin, R. C. Devlin, B. Groever, and F. Capasso, Metasurface Polarization Optics: Independent Phase Control of Arbitrary Orthogonal States of Polarization, *Phys. Rev. Lett.* **118**, 113901 (2017).
- [28] R. Zhao, B. Sain, Q. Wei, C. Tang, X. Li, T. Weiss, L. Huang, Y. Wang, and T. Zentgraf, Multichannel vectorial holographic display and encryption, *Light Sci. Appl.* **7**, 95 (2018).
- [29] A. F. Abouraddy, B. E. A. Saleh, A. V. Sergienko, and M. C. Teich, Quantum holography, *Opt. Express* **9**, 498 (2001).
- [30] F. Devaux, A. Mosset, F. Bassignot, and E. Lantz, Quantum holography with biphotons of high Schmidt number, *Phys. Rev. A* **99**, 033854 (2019).
- [31] R. Chrapkiewicz, M. Jachura, K. Banaszek, and W. Wasilewski, Hologram of a single photon, *Nat. Photonics* **10**, 576 (2016).
- [32] X.-B. Song, D.-Q. Xu, H.-B. Wang, J. Xiong, X. Zhang, D.-Z. Cao, and K. Wang, Experimental observation of one-dimensional quantum holographic imaging, *Appl. Phys. Lett.* **103**, 131111 (2013).
- [33] H. Defienne, B. Ndagano, A. Lyons, and D. Faccio, Polarization entanglement-enabled quantum holography, *Nat. Phys.* **17**, 591 (2021).
- [34] L. Allen, M. W. Beijersbergen, R. J. C. Spreeuw, and J. P. Woerdman, Orbital angular momentum of light and the transformation of Laguerre-Gaussian laser modes, *Phys. Rev. A* **45**, 8185 (1992).
- [35] A. Mair, A. Vaziri, G. Weihs, and A. Zeilinger, Entanglement of the orbital angular momentum states of photons, *Nature (London)* **412**, 313 (2001).
- [36] Q. Zeng, B. Wang, P. Li, and X. Zhang, Experimental High-Dimensional Einstein-Podolsky-Rosen Steering, *Phys. Rev. Lett.* **120**, 030401 (2018).
- [37] Y. Zhang, F. S. Roux, T. Konrad, M. Agnew, J. Leach, and A. Forbes, Engineering two-photon high-dimensional states through quantum interference, *Sci. Adv.* **2**, e1501165 (2016).
- [38] L.-J. Kong, R. Liu, W.-R. Qi, Z.-X. Wang, S.-Y. Huang, Q. Wang, C. Tu, Y. Li, and H.-T. Wang, Manipulation of eight-dimensional Bell-like states, *Sci. Adv.* **5**, eaat9206 (2019).
- [39] B. Wang, T. Chen, and X. Zhang, Experimental Observation of Topologically Protected Bound States with Vanishing Chern Numbers in a Two-Dimensional Quantum Walk, *Phys. Rev. Lett.* **121**, 100501 (2018).
- [40] Y. Shen, X. Wang, Z. Xie, C. Min, X. Fu, Q. Liu, M. Gong, and X. Yuan, Optical vortices 30 years on: OAM manipulation from topological charge to multiple singularities, *Light Sci. Appl.* **8**, 90 (2019).
- [41] X. Fang, H. Ren, and M. Gu, Orbital angular momentum holography for high-security encryption, *Nat. Photonics* **14**, 102 (2020).
- [42] H. Zhou, B. Sain, Y. Wang, C. Schlickriede, R. Zhao, X. Zhang, Q. Wei, X. Li, L. Huang, and T. Zentgraf, Polarization-encrypted orbital angular momentum multiplexed metasurface holography, *ACS Nano* **14**, 5553 (2020).

- [43] See Supplemental Material at <http://link.aps.org/supplemental/10.1103/PhysRevLett.130.053602> for information about the experimental data for certifying the high-dimensional OAM entangled source, OAM-preserved hologram and OAM-selective hologram, the simulation of OAM-selective holography, the quantum OAM-preserved and selective holography, the experimental setup for demonstrating the robustness of our quantum OAM holography, the high-dimensional entangled state for improving the security of quantum OAM holographic encryption in practical application, which includes Refs. [44–48].
- [44] J. P. Torres, A. Alexandrescu, and L. Torner, Quantum spiral bandwidth of entangled two-photon states, *Phys. Rev. A* **68**, 050301(R) (2003).
- [45] R. F. Offer, D. Stulga, E. Riis, S. Franke-Arnold, and A. S. Arnold, Spiral bandwidth of four-wave mixing in Rb vapour, *Commun. Phys.* **1**, 84 (2018).
- [46] J. Bavareco, N. Herrera Valencia, C. Klöckl, M. Pivluska, P. Erker, N. Friis, M. Malik, and M. Huber, Measurements in two bases are sufficient for certifying high-dimensional entanglement, *Nat. Phys.* **14**, 1032 (2018).
- [47] N. Bent, H. Qassim, A. A. Tahir, D. Sych, G. Leuchs, L. L. Sánchez-Soto, E. Karimi, and R. W. Boyd, Experimental Realization of Quantum Tomography of Photonic Qudits via Symmetric Informationally Complete Positive Operator-Valued Measures, *Phys. Rev. X* **5**, 041006 (2015).
- [48] M. A. Nielsen and I. L. Chuang, *Quantum Computation and Quantum Information* (Cambridge University Press, Cambridge, New York, 2000).
- [49] H. Defienne, M. Reichert, J. W. Fleischer, and D. Faccio, Quantum image distillation, *Sci. Adv.* **5**, eaax0307 (2019).
- [50] T. Gregory, P.-A. Moreau, E. Toninelli, and M. J. Padgett, Imaging through noise with quantum illumination, *Sci. Adv.* **6**, eaay2652 (2020).
- [51] M. J. Padgett and J. Courtial, Poincaré-sphere equivalent for light beams containing orbital angular momentum, *Opt. Lett.* **24**, 430 (1999).
- [52] G. Milione, H. I. Sztul, D. A. Nolan, and R. R. Alfano, Higher-Order Poincaré Sphere, Stokes Parameters, and the Angular Momentum of Light, *Phys. Rev. Lett.* **107**, 053601 (2011).
- [53] J. Romero, D. Giovannini, S. Franke-Arnold, S. M. Barnett, and M. J. Padgett, Increasing the dimension in high-dimensional two-photon orbital angular momentum entanglement, *Phys. Rev. A* **86**, 012334 (2012).
- [54] I. Nape, V. Rodríguez-Fajardo, F. Zhu, H.-C. Huang, J. Leach, and A. Forbes, Measuring dimensionality and purity of high-dimensional entangled states, *Nat. Commun.* **12**, 5159 (2021).